Characteristic Impedance Extraction Using Calibration Comparison

Servaas Vandenberghe, Dominique M. M.-P. Schreurs, *Member, IEEE*, Geert Carchon, *Student Member, IEEE*, Bart K. J. C. Nauwelaers, *Senior Member, IEEE*, and Walter De Raedt

***Abstract*—A robust line impedance identification method is presented in this paper. It determines the characteristic impedance of on-wafer thru–line–reflect (TLR) standards measured after an initial off-wafer line–reflect–match or TLR calibration. The only assumption made is that the obtained trans-wafer error boxes are a cascade of a symmetric probe-related disturbance and a change in reference impedance. The proposed method yields an unbiased estimate of the complex characteristic impedance. Results from coplanar lines on a medium resistivity silicon substrate support the made assumption.**

***Index Terms*—Coplanar waveguides, impedance measurement.**

I. Introduction

THE thru–line–reflect (TLR) method is often the most feasible on-wafer calibration technique since it only requires two lines of a different length [1]. A drawback is that the recovered reflection parameters are at an unknown reference impedance, set by the characteristic line impedance. An indirect determination using the propagation constant is only possible for low-loss substrates [2].

Calibration comparison methods measure on-wafer TLR standards after an initial off-wafer calibration at a known reference impedance. The obtained trans-wafer error boxes are then identified with an equivalent circuit, modeling the contact geometry and substrate change, and a transformer [3], [4]. This transformer accounts for the change in voltage over the virtual two-port junction if the reference impedance at both ports is chosen equal. An example is the waveguide TE_{10} E-plane step junction [5, p. 162], where the port impedance is chosen and the modal voltage is determined from power consistency. For ideal transmission-line discontinuities, it is, however, more physically consistent to assume a constant voltage over the junction. This condition determines the port 2 modal voltage, reference impedance, and removes the transformer.

Both interpretations result in the same voltage normalized S-parameter values if the transformer ratio $n = \sqrt{Z_l/Z_s}$. The normalization follows implicitly from the reciprocity condition $S_{n21} = S_{n12}$ as

$$\frac{Y_{21}}{Y_{12}} = 1 \Rightarrow \frac{S_{n21}}{S_{n12}} = \frac{S_{21}\sqrt{\dfrac{Z_{c1}}{Z_{c2}}}}{S_{12}\sqrt{\dfrac{Z_{c2}}{Z_{c1}}}} = 1 \tag{1}$$

shows.

II. Reciprocity

Reciprocity of a two-port junction is a necessary condition for the determination of the forward and reverse transmission if only their product is known, as obtained from, e.g., short–open–load (SOL) or TLR calibration techniques. Equating both quantities [5, p. 159] is not always valid [6].

The voltage S-parameter circuit representation is a compact way of describing an underlying field problem. A normalization relates the field with a macroscopic incident and reflected voltage or current. For TE or TM modes in a reciprocal uniform medium, the fields at port i satisfy [5, p. 72]

$$\begin{aligned}\left[\vec{E}_i, \vec{H}_i\right] = {} & \left[\vec{e}_{ti} + \vec{e}_{zi}, \vec{h}_{ti} + \vec{h}_{zi}\right] C_{0i}^{+} e^{-\gamma z} \\ & + \left[\vec{e}_{ti} - \vec{e}_{zi}, -\vec{h}_{ti} + \vec{h}_{zi}\right] C_{0i}^{-} e^{\gamma z}\end{aligned} \tag{2}$$

with $\vec{e}$, $\vec{h}$ being the z-independent modal fields and C_0^+, C_0^- being the two wave amplitude constants. An arbitrary transversal field follows from

$$\vec{E}_{ti} = \left(\frac{V_{0i}^{+}}{V_{ci}} e^{-\gamma_i z} + \frac{V_{0i}^{-}}{V_{ci}} e^{\gamma_i z}\right) \vec{e}_{ti} = \frac{V_i(z)}{V_{ci}} \vec{e}_{ti} \tag{3}$$

$$\vec{H}_{ti} = \left(\frac{I_{0i}^{+}}{I_{ci}} e^{-\gamma_i z} - \frac{I_{0i}^{-}}{I_{ci}} e^{\gamma_i z}\right) \vec{h}_{ti} = \frac{I_i(z)}{I_{ci}} \vec{h}_{ti} \tag{4}$$

with V_c and I_c being the modal voltage and current. The wave voltages at port i, V_0^+ and V_0^- determine the field since

$$Z_{ci} = \frac{V_{ci}}{I_{ci}} = \frac{V_{0i}^{+}}{I_{0i}^{+}} = \frac{V_{0i}^{-}}{I_{0i}^{-}} \tag{5}$$

holds from (2).

The Lorentz reciprocity theorem [5, pp. 57–59, 159] applied on a two-port source-free junction, e.g., Fig. 1, imposes a condition on the incident and reflected fields. The Lorentz integral

$$\oint_A \left(\vec{E}^I \times \vec{H}^{II} - \vec{E}^{II} \times \vec{H}^I\right) \mathrm{d}\vec{A} = 0 \tag{6}$$

reduces to the two terminal planes if the remaining enclosing surface is characterized by a scalar surface impedance or is in-

Manuscript received March 29, 2001; revised August 23, 2001. The work of S. Vandenberghe was supported by the Institute for the Promotion of Innovation by Science and Technology in Flanders. The work of D. Schreurs was supported by the Fund for Scientific Research.

S. Vandenberghe, D. M. M.-P. Schreurs, and B. K. J. C. Nauwelaers are with the Department of Electronics, Systems, Automation, and Technology-Division TELEMIC, Katholieke Universiteit Leuven, B-3001 Leuven, Belgium (e-mail: Servaas.Vandenberghe@esat.Kuleuven.ac.be).

G. Carchon and W. De Raedt are with the Division Materials, Components, and Packaging–High-Density Interconnect and Packaging Group, Interuniversity Microelectronics Centre, B-3001 Leuven, Belgium.

Publisher Item Identifier S 0018-9480(01)10427-8.

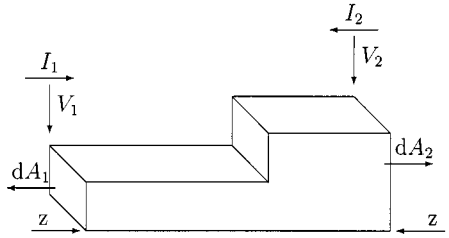

Fig. 1. TE_{10} E-plane step waveguide junction as an example of a reciprocal microwave circuit.

finitely far away. Choosing current sources outside of the junction such that $\vec{E}_{t2}^{I} = 0$, experiment I, and such that $\vec{E}_{t1}^{II} = 0$, experiment II, and substituting with (3)–(4) yields a reciprocity factor

$$K_i = \frac{1}{V_{ci} I_{ci}} \int_{A_i} \vec{e}_{ti} \times \vec{h}_{ti} \cdot \vec{u}_z \, \mathrm{d}A \tag{7}$$

and with (5) results in

$$\frac{Y_{21}}{Y_{12}} = \frac{K_1}{K_2} \Leftrightarrow D = \frac{S_{21}}{S_{12}} = \frac{Z_{c2} K_1}{Z_{c1} K_2} \tag{8}$$

which agrees with [6, eq. (22)]. The Z_c dependence of the reciprocity ratio D is removed using the normalized quantities $V_n^{\pm} = V^{\pm}/\sqrt{Z_c}$, which yields

$$D_n = \frac{S_{n21}}{S_{n12}} = \frac{S_{21}\sqrt{\dfrac{Z_{c1}}{Z_{c2}}}}{S_{12}\sqrt{\dfrac{Z_{c2}}{Z_{c1}}}} = \frac{K_1}{K_2} \tag{9}$$

with S_n the "voltage" normalized S-parameters. Note that calculating $S_{n21} = S_{n12} = \sqrt{S_{21} S_{12}}$ implicitely chooses $V_n^{\pm} = V^{\pm}/\sqrt{Z_c/K}$.

The power carried by the forward modal field agrees with the macroscopic voltage current power if

$$S_{ci} = \frac{1}{2} \int_{A_i} \vec{e}_{ti} \times \vec{h}_{ti}^{\,*} \cdot \vec{u}_z \, \mathrm{d}A = \frac{1}{2} V_{ci} I_{ci}^{*} \tag{10}$$

holds. This power consistency determines the phase of Z_c [7] and sets K_i to unity for TE or TM modes if $[V_c, I_c]$ are in-phase with $[\vec{e}_t, \vec{h}_t]$. A line integral defining V_c or a contour integral defining I_c, for TM or TE modes, in the z-plane satisfies this condition.

III. Error Box Normalization

A trans-wafer error box relates an off- to on-wafer calibration. The reciprocity ratio is calculated assuming an initial coaxial calibration. Performing an off- and on-wafer calibration determines two sets error boxes, i.e., S_x^I and S_x^{II} with $x = [a, b]$, and two sets deembedded S-parameters, i.e., S_D^I and S_D^{II}. The data satisfies

$$S_D^{\mathrm{coax}} = S_a^I || S_D^I || \overline{S_b^I} = S_a^{II} || S_D^{II} || \overline{S_b^{II}} \tag{11}$$

with $||$ being the cascade operator, the reversing overbar as

$$\overline{S} = \begin{bmatrix} 0 & 1 \\ 1 & 0 \end{bmatrix} S \begin{bmatrix} 0 & 1 \\ 1 & 0 \end{bmatrix} \tag{12}$$

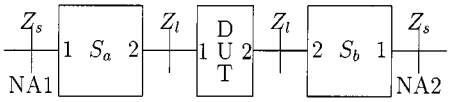

Fig. 2. TLR error-box port numbering. The port 2 reference impedance is set by the line impedance.

and the port numbering from Fig. 2. Rewriting (11) gives

$$S_D^I = 1/S_a^I || S_a^{II} || S_D^{II} || \overline{S_b^{II}} || 1/\overline{S_b^I} \tag{13}$$

with $1/S$ being the S-parameter deembedding matrix. The matrices

$$S_a = 1/S_a^I || S_a^{II} \quad S_b = 1/S_b^I || S_b^{II} \tag{14}$$

describe the on- to off-wafer S-parameter transformation. The reciprocity ratio of these trans-wafer error boxes is

$$D_x = \frac{S_{x21}}{S_{x12}} = \frac{D_x^{II}}{D_x^I} = \frac{K_{x2}^I}{K_{x2}^{II}} \tag{15}$$

using the port numbering in Fig. 2 and the normalization from (9). The ratio D_x is unity if the off- and on-wafer factors K are equal, and is independent of the coax calibration.

Linear calibration algorithms, e.g., TLR and line–reflect–match (LRM), recover the reflection coefficients and an estimate of

$$S_{a21} S_{a12} \approx k_1$$
$$S_{b21} S_{b12} \approx k_2 \tag{16}$$
$$S_{a21} S_{b12} \approx k_3$$
$$S_{b21} S_{a12} \approx k_4 \tag{17}$$

for the transmission coefficients [8]. The ratio

$$\frac{D_b}{D_a} \approx \frac{k_4}{k_3} \tag{18}$$

is also determined. This seven-term linear calibration is converted into an eight-term absolute calibration through the estimation of one factor. A solution, for reciprocal error boxes with a reciprocity ratio of unity, is to determine S_{a21} such that $D_a \approx 1 \approx D_b$, thus choosing voltage normalized S-parameters. An exact solution requires that (18) equals unity. A practical approach is to distribute the error over D_a and D_b using

$$D_a D_b = 1 \Rightarrow D_a = s_1 \sqrt{k_3/k_4} \tag{19}$$
$$\Rightarrow S_{a21} = s_2 \sqrt{k_1 D_a}. \tag{20}$$

The sign $s_i = \pm 1$ is chosen such that the obtained value approximates $e^{-j\omega\tau_i}$, where τ_i is an adaptive estimation from previous frequency points with an initial value zero. The reciprocity error $|D_x - 1|$ is typically lower than 10^{-3} for good measurements.

IV. Error Box Identification

The trans-wafer error box $x = \{a, b\}$ is modeled by a symmetric probe related disturbance S_{xp} cascaded by a change in

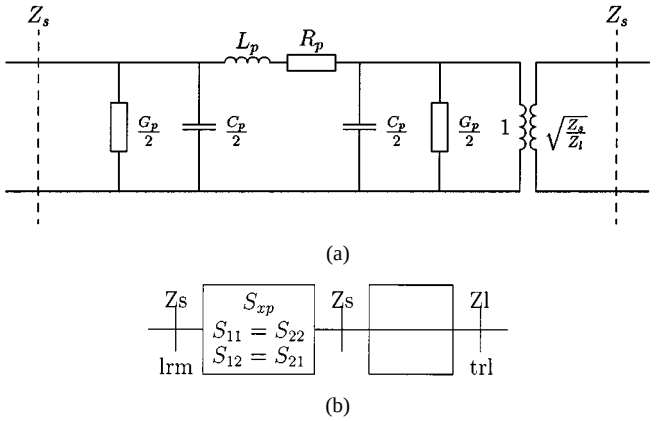

Fig. 3. Error-box model used for the characteristic impedance identification. (a) Equivalent circuit. (b) Reflection-parameter-based model. The S-parameter response follows from the cascade of a symmetric probe related disturbance S_{xp} and an impedance change from Z_s to Z_l.

reference impedance from Z_s to Z_l (see Fig. 3). The S-parameters follow from

$$S_x^{\text{cir}} = \begin{bmatrix} S_{xp11} & S_{xp12} \\ S_{xp12} & S_{xp11} \end{bmatrix} || S_z(Z_s, Z_l) \tag{21}$$

$$S_z = \frac{1}{Z_{02} + Z_{01}} \cdot \begin{bmatrix} Z_{02} - Z_{01} & 2\sqrt{Z_{01}Z_{02}} \\ 2\sqrt{Z_{01}Z_{02}} & -Z_{02} + Z_{01} \end{bmatrix} \tag{22}$$

with $S_z(Z_{01}, Z_{02})$ being the response of a thru in a Z_{01}/Z_{02} environment. Equating simulated and measured S-parameters for M error boxes yields $8M$ real equations

$$\vec{f}(\vec{x}) = \begin{bmatrix} \vdots \\ \Re(S_{xij}^{\text{cal}} - S_{xij}^{\text{cir}}) \\ \Im(S_{xij}^{\text{cal}} - S_{xij}^{\text{cir}}) \\ \vdots \end{bmatrix} = \vec{0} \tag{23}$$

of which $6M$ is independent due to reciprocity. There are $4M+2$ real unknowns since Z_s is known and Z_l is equal for all error boxes.

The linearization of $\vec{f}(\vec{x})$ in the solution reveals the sensitivity information. The Jacobian is rewritten as $J = USV^T$ by the singular value decomposition, with $U = [\ldots \vec{u}_i \ldots]$ and $V = [\ldots \vec{v}_i \ldots]$ being orthonormal and S being a diagonal matrix of singular values s_i. From

$$\Delta\vec{f} \approx J\Delta\vec{x} = USV^T\Delta\vec{x} \tag{24}$$

it follows that the penalty $||\Delta\vec{f}||$ for adding $\vec{v}_i$ to the solution is given by $||J\vec{v}_i|| = s_i$. Table I summarizes the results for one trans-wafer error-box modeling a coplanar waveguide (CPW) discontinuity at 10 GHz. The estimation of Z_l is decoupled from the probe parasitics S_{xp}, which is true as long as the probe disturbance is small. The singular values indicate that $\vec{f}$ is more sensitive for the probe-related unknowns. A noticeable faster convergence of the Newton–Rhapson zero solving algorithm for S_{xp}, compared to Z_l, may thus be explained.

TABLE I
VECTORS $\vec{v}_i$ AND THEIR ASSOCIATED SINGULAR VALUE FOR THE LINEARIZED ONE ERROR BOX IDENTIFICATION PROBLEM. MEASURED S-PARAMETERS AT 10 GHz FROM THE STRUCTURES IN FIG. 10 WERE USED. THE IDENTIFIED EXACT SOLUTION IS $Z_l = 51.7 + j7.6\,\Omega$, $S_{ap11} = -0.01 - j0.01$ AND $S_{ap12} = 0.98 - j0.02$, IF $Z_s = 50\,\Omega$

$\vec{x} =$	$\vec{v}_1$	$\vec{v}_2$	$\vec{v}_3$	$\vec{v}_4$	$\vec{v}_5$	$\vec{v}_6$
$\Re(Z_l)$					-1.0	
$\Im(Z_l)$						-1.0
$\Re(S_{ap11})$	.17	.65	$-.72$	.20		
$\Im(S_{ap11})$	$-.65$	.17	.20	.72		
$\Re(S_{ap12})$	.20	.72	.65	$-.17$		
$\Im(S_{ap12})$	$-.72$	.20	$-.17$	$-.65$		
s_{ii}	1.5	1.5	1.4	1.4	0.01	0.01

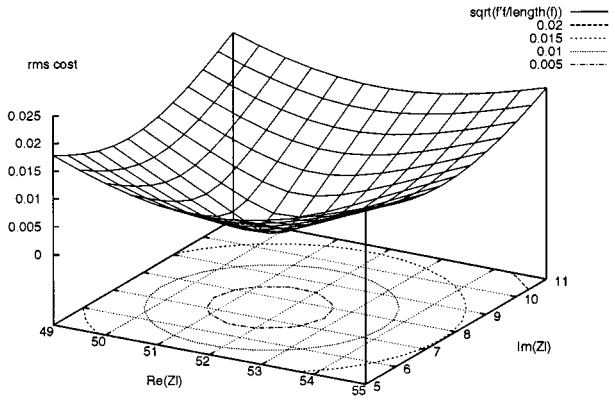

Fig. 4. rms cost of the bidirectional search method. A clear distinct minimum with equal sensitivity for the real and imaginary parts is centered around the least squares solution $Z_l = 51.7 + j7.6$. The two error-box experimental data are from the structures in Fig. 10 at 10 GHz.

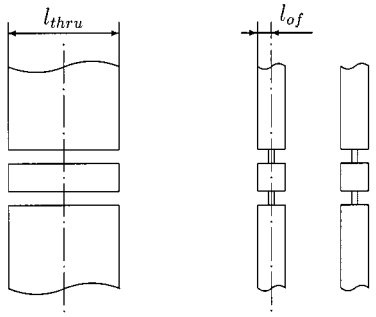

Fig. 5. Typical probe standards present on a coplanar LRM calibration substrate. The recovered S-parameters are: (a) at a reference plane in the center of the thru. The reference impedance is set by: (b) the probe-tip load response calculated at the reference plane.

V. BIDIRECTIONAL SEARCH

The iterative solution of $\vec{f}(\vec{x}) = \vec{0}$ searches for all unknowns simultaneously and is a forward-search method. Direct-extraction backward-search methods calculate unknown per unknown from selected measurements. A bidirectional-search approach

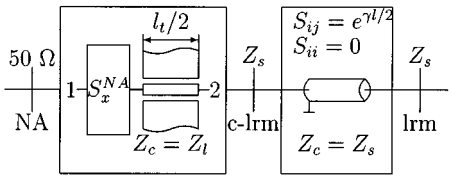

Fig. 6. Probe-tip LRM calibration corrects for a nonzero-length thru by shifting the reference plane from the center of the thru to the probe tip. Numerically, the zero-length thru error box (left-hand side) is cascaded by a negative delay transmission line (right-hand side). This correction is approximative if $Z_s \neq Z_l$, but does not change the reference impedance Z_s.

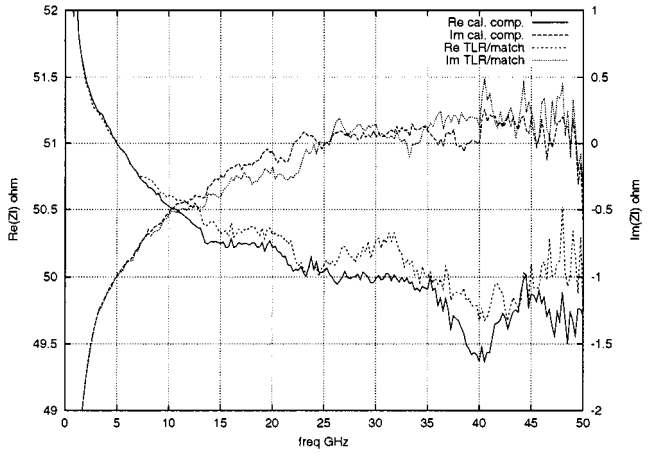

(a)

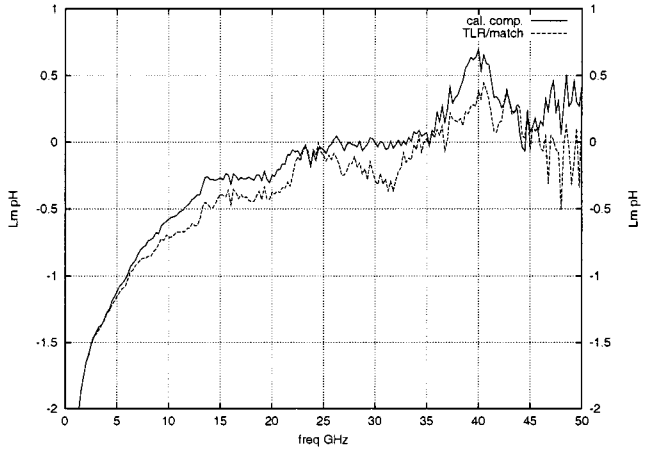

(b)

Fig. 7. (a) Extracted line impedance using the new technique and the TLR/match method. (b) Series inductance of the virtual load at the reference plane in the center of a 197.4-μm thru with $l_{of} = 25.4$ μm for the two methods. This inductance models the probe tip to reference plane offset error. The load itself is assumed equal to 50 Ω. The error boxes were calculated using an initial probe-tip LRM calibration as a reference, followed by a multiline TLR on the same alumina calibration substrate.

[9] was implemented to exploit the sensitivity difference and to reduce the number of unknowns from $4M + 2$ to 2. The line impedance Z_l is the ordinary optimization unknown, and the probe disturbance is extracted as follows: for every port x

1) calculate S_z and $S_{z,\,\mathrm{inv}} = S_z(Z_l,\, Z_s)$ from Z_l, with $\vec{x} = [\Re(Z_l); \Im(Z_l)]$;
2) recover the probe response from the measurements S_x^{cal} using $S_{xp}^{\mathrm{rec}} = S_x^{\mathrm{cal}} || S_{z,\,\mathrm{inv}}$;

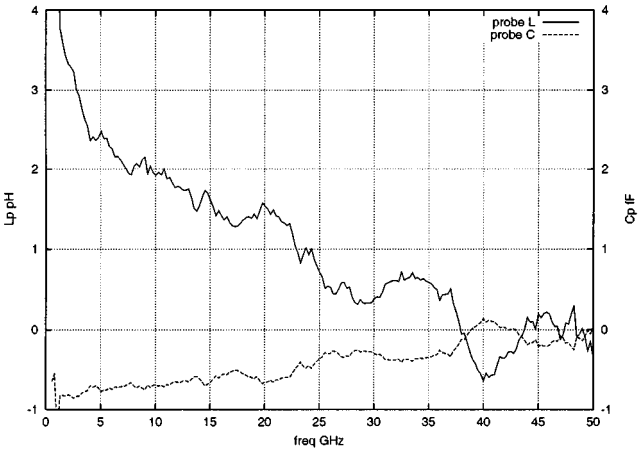

Fig. 8. Extracted probe L and C, averaged over error box a and b, for the LRM/TLR trans-calibration error boxes. The probe-tip LRM and TLR were performed on the same alumina calibration substrate. Remaining parasitics result from the approximate probe-tip LRM and measurement error.

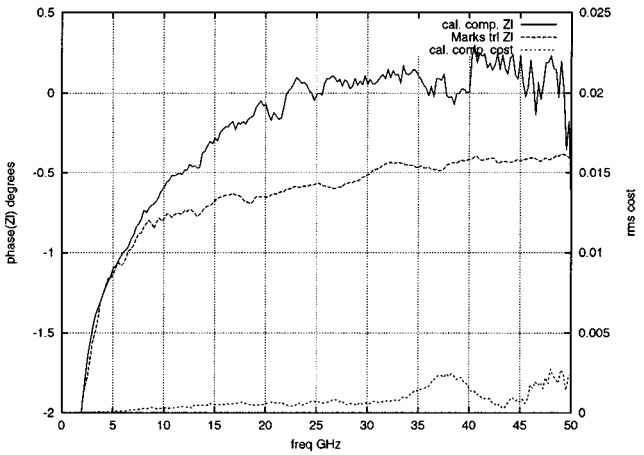

Fig. 9. Comparison of the phase of the extracted line impedance using the new technique and the propagation constant method. The rms S-parameter difference between the model and measurement is also shown. The TLR standards consist of six CPW lines (50/25/200 μm strip/slot/ground-plane wide and 197.4, 432.9, 870.9, 1736.8, 1736.8, 3383.1, 5080 μm long) fabricated on an alumina substrate. An initial probe-tip LRM calibration was used as a reference.

3) extract a better estimate with

$$S_{xp11}^{\mathrm{est}} = (S_{xp11}^{\mathrm{rec}} + S_{xp22}^{\mathrm{rec}})/2 \tag{25}$$

$$S_{xp12}^{\mathrm{est}} = (S_{xp12}^{\mathrm{rec}} + S_{xp21}^{\mathrm{rec}})/2; \tag{26}$$

4) calculate $S_x^{\mathrm{cir}} = S_{xp}^{\mathrm{est}} || S_z$;
5) evaluate (23) and add the eight results to $\vec{f}$.

Repeating this procedure M times yields $8M$ equations. The condition of the linearized problem reduces to unity, indicating equal sensitivity for the real and imaginary parts of Z_l. The internal condition is, however, unchanged and the probe-related unknowns are still extracted with higher accuracy. The cost function for two trans-wafer error boxes (Fig. 4) shows a well-defined minimum. Robustness and convergence speed improve due to the efficient estimation (25) of the usually low probe reflections.

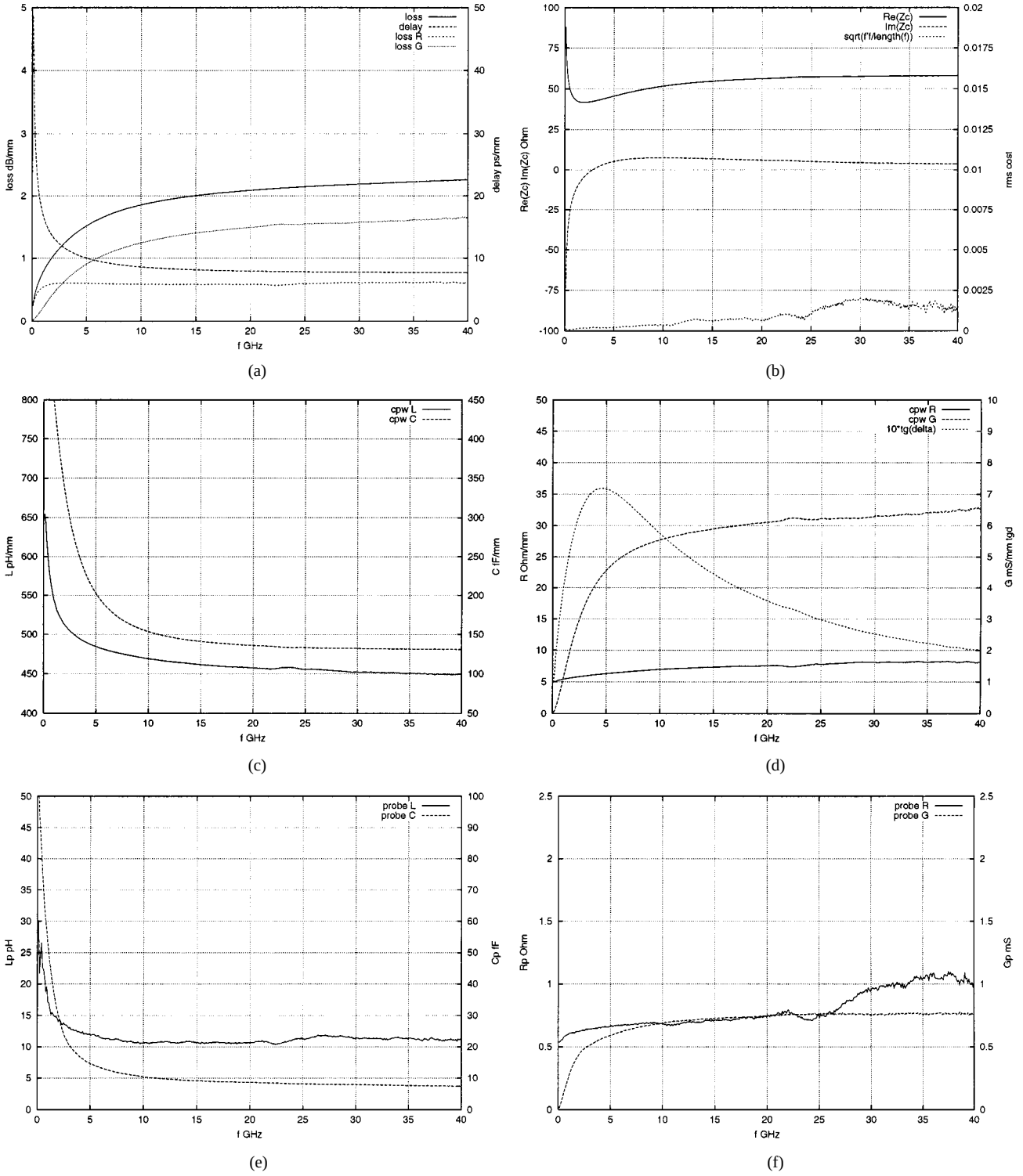

Fig. 10. (a) Line loss, delay, and the series and parallel loss calculated from the telegrapher's equation. (b) Estimated line impedance and error-box fit cost. (c), (d) Extracted line L, C and R, G, $\mathrm{tg}\delta$. (e), (f) Total extracted probe L, C and R, G averaged over error box a and b. All plots are for 0.5-μm-thick Al 15/11/183 μm coplanar lines separated from a 5-S/m Si substrate by a 1-μm-thick dielectricum. The lines were 100-, 340-, 1300-, and 6300-μm long.

VI. LRM Offset Compensation

Calibration comparison methods rely on the accurate knowledge of the off-wafer reference impedance Z_s since only the ratio Z_l/Z_s is independently estimated as follows from, for example, (22). Off-wafer LRM is broad band, but high-frequency accuracy is limited by the imperfect match standard. Moreover, most coplanar calibration substrates use a nonzero-length thru combined with probe-tip loads, as shown in Fig. 5. This offset change introduces an error if the thru line and load impedance differ. The LRM algorithm employs a match standard to determine the error-box port-1 reflection S_{x11} (see Fig. 2). Further completion establishes a port-2 reference plane in the center of the thru if its delay is assumed to be zero. By definition, the calibration reference impedance Z_s is the load by which port 2 is

terminated such that the input reflection equals S_{x11}. Thus, Z_s is the match impedance Z_m recalculated at the reference plane.

A probe-tip LRM calibration uses a specified delay and loss to shift the reference plane from the center of the thru to the probe tip. The thru is assumed reflection free and fully characterized by its total propagation constant γl. Actually, the algorithm cascades the zero length thru error box (see Fig. 6) by a negative delay transmission line at port 2. The zero reflection assumption sets the characteristic impedance of this line equal to Z_s. This correction is approximative if the thru line impedance Z_l differs from Z_s, yielding remnant probe parasitics, but the reference impedance remains unchanged.

In both cases, the LRM reference impedance Z_s equals the match impedance Z_m calculated at the reference plane in the center of the thru. For a probe tip-load, Z_s follows from a cascade of a negative length thru line terminated in Z_m. The match impedance $Z_m(z=0)$ relates to $Z_s(z)$ measured at position z along the thru line using the deembedding formula

$$z_m = \frac{Z_m}{Z_l} = \frac{z_s + \mathrm{tgh}(\gamma z)}{1 + z_s \mathrm{tgh}(\gamma z)} \tag{27}$$

with

$$z_s = \frac{Z_s}{Z_l}, \qquad z = -(l_{of} - l_{thru}/2). \tag{28}$$

The unknowns γ and z_s are obtained from an LRM followed by a TLR calibration on the same wafer, with all lines equal in transverse geometry. Impedance identification applied on these LRM-to-TLR trans-calibration error boxes yields z_s and z_m via (27). The estimation of Z_l via Z_m/z_m is independent of the offset error between the match and the thru reference plane. A virtual load response Z_s then follows from z_s.

An alternative approach is to perform a TLR calibration and to contact the match standard. This TLR/match method measures the normalized impedance z_m, and z_s then follows from (27). Both methods allow for the determination of Z_l and Z_s if Z_m is known.

VII. Experiment

The network analyzer was calibrated by an off-wafer probe-tip LRM calibration on a Cascade 101-190 coplanar alumina substrate. The thru loss and delay, i.e., 32 G $\cdot\,\Omega$/s and 1.13 ps, were estimated from the available lines. A multiline TLR was used to calculate the LRM-to-TLR error boxes. The effect of the match offset error was estimated by setting the probe-tip load to 50 Ω (see Fig. 7). The resulting error, a load inductance of about -0.5 pH around 14 GHz, is limited to $j0.04\,\Omega$ below 35 GHz. Agreement of the results from the new and TLR/match method supports the made assumptions. Also, the low probe parasitics present in the LRM/TLR trans-calibration error boxes show that the probe-tip LRM, although approximative, is quite accurate (see Fig. 8).

A comparison of the line-impedance phase estimated from the new technique and the propagation constant method of [2] (see Fig. 9) validates the new approach for low-loss substrates.

The remaining difference may result from an inadequate error-box model (here, probably above 35 GHz), an increase in dielectric loss, assumed zero in [2], or non-TE or non-TM behavior, which invalidates (1).

The on-wafer calibration structures consist of 0.5-μm-thick Al 15/11/183 μm, strip/slot/ground plane, coplanar lines of 100-, 340-, 1300-, and 6300-μm long, separated by a 1-μm-thick dielectricum from a 5-S/m Si lossy substrate. Multiline TLR was performed to obtain the error-box data. Fig. 10 summarizes the results, which are consistent with [10]. Especially the low-frequency *RC* behavior, up to 1 GHz, and the high loss transition between the slow-wave and dielectric quasi-TEM mode, at 3 GHz, is clearly visible.

The series and parallel loss was calculated from

$$\gamma = \sqrt{(R + j\omega L)(G + j\omega C)} \tag{29}$$

$$\approx \frac{R}{2\Re(Z_l)} + \frac{G\Re(Z_l)}{2} + j\omega\sqrt{LC} \tag{30}$$

which holds if $\omega L \gg R$ and $\omega C \gg G$ since

$$Z_l = \sqrt{\frac{R + j\omega L}{G + j\omega C}} \tag{31}$$

$$\approx \sqrt{\frac{L}{C}}\left[1 + j\left(\frac{G}{2\omega C} - \frac{R}{2\omega L}\right)\right] \tag{32}$$

is then valid. The error in (30), for the data presented here, is below 1.5% above 1 GHz.

VIII. Conclusion

A robust line-impedance identification method has been presented in this paper. The method compares two calibrations and assumes that the difference is a symmetric error. Thus, any nonsymmetry is attributed to a reference impedance change. The method is reflection parameter based and avoids any transformation into chain or transmission parameters.

Acknowledgment

The authors wish to acknowledge D. Vanhoenacker, Université Catholique de Louvain, Louvain-La-Neuve, Belgium, for making available the measurements used to develop the technique discussed in this paper. The reported data is from a silicon wafer designed and processed by the Interuniversity Microelectronics Centre (IMEC), Leuven, Belgium.

References

[1] M. B. Marks, "A multiline method of network analyzer calibration," *IEEE Trans. Microwave Theory Tech.*, vol. 39, pp. 1205–1215, July 1991.

[2] R. Marks and D. Williams, "Characteristic impedance determination using propagation constant measurement," *IEEE Microwave Guided Wave Lett.*, vol. 1, pp. 141–143, June 1991.

[3] G. Carchon, D. Schreurs, S. Vandenberghe, B. Nauwelaers, and W. De Raedt, "Compensating differences between measurement and calibration wafer in probe tip calibrations—Deembedding of line parameters," in *Eur. Microwave Conf.*, Amsterdam, The Netherlands, Oct. 1998, pp. 259–264.

[4] D. Williams, U. Arz, and H. Grabinski, "Accurate characteristic impedance measurement on silicon," in *IEEE MTT-S Int. Microwave Symp. Dig.*, 1998, pp. 1917–1920.
[5] R. Collin, *Foundations for Microwave Engineering*. New York: McGraw-Hill, 1966.
[6] D. Williams and R. Marks, "Reciprocity relations in waveguide junctions," *IEEE Trans. Microwave Theory Tech.*, vol. 41, pp. 1105–1110, June/July 1993.
[7] J. Brews, "Characteristic impedance of microstrip lines," *IEEE Trans. Microwave Theory Tech.*, vol. MTT-35, pp. 30–34, Jan. 1987.
[8] R. Pantoja, M. Howes, J. Richardson, and R. Pollard, "Improved calibration and measurement of the scattering parameters of microwave integrated circuits," *IEEE Trans. Microwave Theory Tech.*, vol. 37, pp. 1675–1680, Nov. 1989.
[9] F. Lin and G. Kompa, "FET model parameter extraction based on optimization with multiplane data-fitting and bidirectional search—A new concept," *IEEE Trans. Microwave Theory Tech.*, vol. 42, pp. 1114–1121, July 1994.
[10] E. Grotelüschen, L. S. Dutta, and S. Zaage, "Quasi-analytical analysis of the broadband properties of multiconductor transmission lines on semiconducting substrates," *IEEE Trans. Comp., Packag., Manufact. Technol. B*, vol. 17, pp. 376–382, Aug. 1994.

Servaas Vandenberghe was born in Leuven, Belgium, on March 31, 1972. He received the M.Sc. degree in electrical engineering from the Katholieke Universiteit (K.U.) Leuven, Leuven, Belgium, in 1996, and is currently working toward the Ph.D. degree.

His main research interest is equivalent-circuit-based nonlinear high electron-mobility transistor (HEMT) modeling.

Dominique M. M.-P. Schreurs (S'90–M'97) received the M.Sc. degree in electronic engineering and the Ph.D. degree (*summa cum laude*) from the Katholieke Universiteit (K.U.) Leuven, Leuven, Belgium, in 1992 and 1997, respectively.

She is currently a Post-Doctoral Fellow and a Visiting Assistant Professor at the K.U. Leuven. Her main research interest is the use of vectorial large-signal measurements for the characterization and modeling of nonlinear microwave devices.

Geert Carchon (S'97) was born in Gent, Belgium, on June 14, 1973. He received the M.Sc. and Ph.D. degrees in electrical engineering from the Katholieke Universiteit (K.U.) Leuven, Leuven, Belgium in 1996 and 2001, respectively.

From 1997 to 2000, he was a Research Assistant at the Flemish Institute for the Advancement of Scientific Technological Research in Industry (IWT). Since 2001, he has been with the Division Materials Components, and Packaging–High Density Interconnect and Packaging Group, Interuniversity Microelectronics Centre (IMEC), Leuven, Belgium. His main interests include the measurement, characterization, and modeling of passive devices, and the design of RF and microwave circuits in monolithic microwave integrated circuits (MMICs), and multilayer multichip modules (MCM-Ds).

Bart K. J. C. Nauwelaers (S'80–M'86–SM'99) was born in Niel, Belgium, on July 7, 1958. He received the M.S. and Ph.D. degrees in electrical engineering from the Katholieke Universiteit (K.U.) Leuven, Leuven, Belgium, in 1981 and 1988, respectively, and the Mastère degree from the Ecole Nationale Supérieure des Télécommunications (ENST), Paris, France.

Since 1981, he has been with the Electronics, Systems, Automation, and Technology (ESAT) Laboratory, K.U. Leuven, where he has been involved in research on microwave antennas, microwave integrated circuits and MMICs, and wireless communications. He also teaches courses on microwave engineering, analog and digital communications, and design in electronics and telecommunications.

Walter De Raedt received the M.Sc. degree in electrical engineering from the Katholieke Universiteit (K.U.) Leuven, Leuven, Belgium, in 1981.

He subsequently joined the Electronics, Systems, Automation, and Technology (ESAT) Laboratory, K.U. Leuven, as a Research Assistant, where he was involved with electron-beam lithography. In 1984, he joined the Interuniversity Microelectronics Centre (IMEC), Leuven, Belgium, where he began his involvement with advanced submicrometer III–V devices and MMICs. His current research activities are oriented toward microwave MCM-D systems.